Supporting information

Partially Naked Fluoride in Solvate Ionic Liquids

Zhengfei Chen,[a] Yuto Tonouchi,[a] Kazuhiko Matsumoto,[a] Masayuki Saimura,[b] Rob Atkin,[c] Takashi Nagata,[b] Masato Katahira,[b] and Rika Hagiwara[a]*

[a]Department of Fundamental Energy Science, Graduate School of Energy Science, Kyoto University, Yoshida, Sakyo-ku, Kyoto 606-8501, JAPAN

[b]Institute of Advanced Energy, Kyoto University, Uji, Kyoto 611-0011, JAPAN

[c]School of Molecular Sciences, The University of Western Australia, 35 Stirling Highway, Perth, WA 6009, Australia

Corresponding Author

*k-matsumoto@energy.kyoto-u.ac.jp (Kazuhiko Matsumoto)

Experimental Procedures

Materials. All non-volatile materials were handled in a drybox under an atmosphere of dry Ar. The starting bromides, 1-ethyl-3-methylimidazolium bromide ($[C_2C_1im]Br$) and 1-buthyl-3-methylimidazolium bromide ($[C_4C_1im]Br$), were purchased from Kanto Chemical Co. Inc. and were dried under vacuum at 50 °C overnight. Dry ethylene glycol (EG) (Wako Pure Chemicals, water content < 30 ppm) and methanol (Wako Pure Chemicals, water content < 10 ppm) were used without further purification. Silver fluoride (Aldrich, 99% purity) was further dried under vacuum overnight at 100 °C. Benzyl bromide (98%) and 1,3,5-trifluorobenzene (97%) were purchased from Wako Pure Chemicals and used as received.

Synthesis of $[C_2C_1im]F{\cdot}EG$. In dry methanol, 3.821 g of $[C_2C_1im]Br$ (20.01 mmol) and 2.537 g of AgF (20.01 mmol) were reacted for 30 min, and 1.241 g of dry EG (20.00 mmol) was added onto it. The reaction mixture was stirred for 24 h and the solid precipitate was filtered. The methanol in the clear filtrate was removed under vacuum overnight at 25°C and the final vacuum reached around 1 Pa. The final product typically resulted in a slightly yellow and viscous liquid (~3.0 g). ^{1}H NMR (600 MHz, neat): δ $C_2C_1im^+$: 0.66 (s,3H), 3.37 (s,3H), 3.64 (s,2H), 7.73 (s,3H), 9.92 (s, br). EG: 2.68 (s,4H), 7.73 (s, br,3H). ^{19}F NMR (564 MHz, neat): δ -112.9 (s).

Synthesis of $[C_4C_1im]F{\cdot}EG$. The same procedure as that for $[C_2C_1im]F{\cdot}EG$ was used. Reaction of 4.382 g of $[C_4C_1im]Br$ (20.00 mmol), 2.357 g of AgF (20.01 mmol), and 1.241 g of dry EG (20.00 mmol) gave a yellow and viscous liquid (~3.0 g). ^{1}H NMR (600 MHz, neat): δ $C_2C_1im^+$: 0.08 (s,3H), 0.52 (s,2H), 1.11 (s,2H), 3.42 (s,3H), 3.71 (s,2H), 7.71 (s,br), 7.85 (s,br), 10.13 (s, br). EG: 2.83 (s,4H), 7.82 (s, br). ^{19}F NMR (564 MHz, neat): δ -112.0 (s).

Synthesis of [C_2C_1im]Br·EG. 3.821 g of [C_2C_1im]Br (20.01 mmol) and 1.241 g of dry EG (20.00 mmol) was directly mixed and was stirred for 1 h and the resulting product was clear liquid. ^{1}H NMR (600 MHz, neat): δ $C_2C_1im^+$: 0.66 (s,3H), 3.27 (s,3H), 3.59 (s,2H), 7.14 (s,1H), 7.27 (s,1H), 8.66 (s,1H). EG: 2.69 (s,4H), 3.71 (s,2H).

Synthesis of [C_4C_1im]Br·EG. 4.382 g of [C_2C_1im]Br (20.01 mmol) and 1.241 g of dry EG (20.00 mmol) was directly mixed and was stirred for 1 h and the resulting product was clear liquid.^{1}H NMR (600 MHz, neat): δ $C_2C_1im^+$: 0.04 (s,3H), 0.47 (s,2H), 1.06 (s,2H), 3.32 (s,3H), 3.62 (s,2H), 7.22 (s,1H), 7.34 (s,1H), 8.81 (s,1H). EG: 2.76 (s,4H), 3.78 (s,2H).

Spectroscopic measurements. The impurities of Br and Ag were measured by an Rigaku EDXL 300 X-ray fluorescence spectrometer at operation voltage of 50 kV and current of 2 mA. The intensity of Br was calibrated with [C_2C_1im]Br. The chemical structures of [C_2C_1im]F·EG and [C_4C_1im]F·EG complexes were confirmed by ^{1}H and ^{19}F NMR on a JNM–ECA600 NMR spectrometer (JEOL Ltd.) at various temperatures (up to 60 °C). Neat liquid samples were used for the NMR measurements. A coaxial NMR tube was used with the sample being placed in the internal tube and the deuterated solvent in between to eliminate the interaction with the solvent. The self-diffusion coefficients of the imidazolium cations and EG in the compounds were measured using pulse-gradient spin-echo sequence at 40 and 60°C, and analysed on the basis of the Stejskal equation $\ln E = -D\gamma^2 g^2 \delta^2 (\Delta - \delta/3)$,[1] where E is the echo signal attenuation, D is the self-diffusion coefficient, γ is the gyromagnetic ratio for ^{1}H, g is the amplitude of the gradient pulses (3.0 mT m^{-1}–300.0 mT m^{-1}), δ is the duration of the gradient pulses (2.0 ms), and Δ is the interval between the leading edges of the gradient pulses (100 ms). Infrared spectra were obtained by a Bruker Alpha II spectrometer equipped with an attenuated total reflection setup in a dry chamber (Daikin Industries, LTD.) under a dry air (dew point temperature below –60 °C) at

25° C. A Bruker MultiRAM Raman spectrometer equipped with a liquid N_2-cooled CCD detector was used to record the Raman spectra of the samples sealed in NMR glass tubes.

Single-crystal X-ray diffraction. Single-crystal X-ray diffraction measurements were performed using a R-axis Rapid II diffractometer (Rigaku Corporation) controlled by RAPID AUTO 2.40 software.[2] Crystals of $([C_2C_1im]F)_2$·EG were grown from the supercooled state at 298 K. A selected crystal was sealed in a quartz capillary under a dry air atmosphere and mounted on the diffractometer under a cold dry-nitrogen flow. Data collection was performed at 123 K and consisted of 12 ω scans (130–190°, 5° per frame) at fixed φ (0°) and χ (45°) angles and 32 ω scans (0–160°, 5° per frame) at fixed φ (180°) and χ (45°) angles. The X-ray output was 50 kV–40 mA and the exposure time was 400 s deg^{-1}. Integration, scaling, and absorption corrections were performed using RAPID AUTO 2.40 software. The structure was solved using SIR-92[3] and refined by SHELXL-97[4] linked to Win-GX.[5] Anisotropic displacement factors were introduced for non-hydrogen atoms and hydrogen atoms were treated using an appropriate riding model.

Thermal analysis. Thermal transition temperatures were determined using a Rigaku DSC8230 differential scanning calorimeter. The samples were hermetically sealed in aluminium pans in the drybox. Samples were cooled to -100 °C and then were heated to 80 °C at a scan rate of 5 °C min^{-1} under Ar atmosphere. Thermal decomposition behaviour was analysed by a Rigaku TG-DTA 8120 analyser from room temperature to 400 °C at a heating rate of 10 °C min^{-1} under Ar. Viscosities was measured using an electromagnetically spinning viscometer (EMS-1000, Kyoto Electronics Manufacturing) from 25 to 80 °C. Samples for viscosity measurement were loaded in a glass tube in the drybox and was tightly sealed with a plastic cap. Ionic conductivities at various temperatures were measured with the aid of a Hioki E.E. 3532-80 impedance analyser by

an AC impedance technique using a cell with stainless steel disk electrodes. A standard 0.1 M KCl aqueous solution was used to calibrate the cell. Densities were measured using an oscillating U-tube density meter (DMA 4500M, Anton Paar GmbH).

Fluorination reactions. Benzyl bromide and $[C_2C_1im]F{\cdot}EG$ were directly mixed at 1:1 or 1:1.5 molar ratio in a drybox at room temperature for two hours prior to NMR analysis. Parallel experiments were also conducted in DMF solvent for comparison. Neat reaction solutions were used for ^{1}H NMR to check the conversion rate and the yield of fluoride product (benzyl fluoride) was estimated by ^{19}F NMR using a known amount of 1,3,5-trifluorobenzene as internal standard.[6]

Raman spectroscopic analysis

Raman spectroscopy is more useful than Infrared spectroscopy to identify the conformation of the alkyl chain in $C_nC_1im^+$[7] although it is not sensitive to the OH groups around 3300 cm^{-1}. Characteristic C-C Raman stretching bands resulting from the *gauche* and *trans*-conformations of the alkyl chain to the imidazolium cation have been discussed in literature.[7-10] We particularly focus on the region between 550 and 650 cm^{-1} region in Fig. S13. The bands around 600 and 624 cm^{-1} are identified as *gauche* and *trans*-conformers, respectively, for the butyl chain of the $C_4C_1im^+$ cation. For the $C_2C_1im^+$, two bands at ~600 cm^{-1} and ~624 cm^{-1} are identified as non-planar (ethyl out of the plane of the imidazolium ring) and planar conformations of the cation, respectively, and the non-planar conformer is more stable than the planar conformer in gas phase.[7, 11-12] Consequently, the Raman intensity of the former dominates $C_2C_1im^+$. The likely conformers of *gauche* and *trans* for $C_4C_1im^+$, and non-planar and planar for $[C_2C_1im]$ are presented in supporting information (Fig.S14).

We observe that the area ratio between gauche and trans bands increases from 1.24 of the bromide compound to 1.31 of the fluoride compound, indicating the *gauche* conformation is preferable when the anion is smaller which is in good agreement with literature works.[9-10] When the halide anion is smaller, its electronegativity increases whereas the intermolecular distance is smaller. As a result, the interactions between halide and H(8) on the butyl chain (which are β-H) is stronger, leading to a preferred *gauche* conformations. This is also the same case for the $C_2C_1im^+$ cation that there is an increase in the nonplanar conformation (nonplanar to planar area ratio increases from 3.99 for the bromide compound to 4.24 for the fluoride compound) due to the stronger intermolecular interaction between fluoride and H(7) on the ethyl chain.

Table S1. Fitted VTF parameters of viscosity and ionic conductivity for $[C_2C_1im]F{\cdot}EG$ $[C_4C_1im]F{\cdot}EG$, $[C_2C_1im]B{\cdot}EG$, and $[C_4C_1im]Br{\cdot}EG$.

	$10^3 A_\eta$/mPa s $K^{-1/2}$	B_η/K	T_0/K	$10^{-4} A_\sigma$/mS cm^{-1}	B_σ/K	$T_{0\sigma}$/K
$[C_2C_1im]F{\cdot}EG$	4.9	1152	168	4.35	941	177
$[C_4C_1im]F{\cdot}EG$	2.4	1401	160	4.77	1109	174
$[C_2C_1im]Br{\cdot}EG$	2.4	1098	135	4.85	786	154
$[C_4C_1im]Br{\cdot}EG$	1.2	1381	129	3.30	781	171

Table S2. Crystallographic data for $([C_2C_1im]F)_2 \cdot EG$ (CCDC 1870396).

Salt	$([C_2C_1im]F)_2 \cdot EG$
Formula	$C_{14}H_{28}O_2F_2N_4$
Formula weight	161.20
Crystal system	Triclinic
Space group	*P*-1
a / Å	7.1382(5)
b / Å	8.3988(8)
c / Å	8.9363(6)
V / Å^3	453.96(6)
Z	1
ρ_{calc} / g cm^{-3}	1.179
T / K	113
$R_1(F_o)^a$	0.0468
$wR_2(F_o^2)^b$	0.1425

[a] $R_1 = \Sigma||F_o| - |F_c|| / \Sigma|F_o|$ for $I > 2\sigma(I)$.

[b] $wR_2 = [\Sigma[w(F_o^2 - F_c^2)^2] / \Sigma[w(F_o^2)^2]]c^{1/2}$.

Table S3. Selected bond lengths and angles in $([C_2C_1im]F)_2 \cdot EG$ (Å, °)

N1−C2	1.334(2)	N3−C8	1.462(2)
N1−C5	1.378(2)	C5−C4	1.347(2)
N1−C6	1.473(2)	C6−C7	1.495(3)
N3−C2	1.330(2)	C10−C10^{i}	1.503(4)
N3−C4	1.378(2)	O9−C10	1.411(2)
N1−C6−C7	112.08(15)	C4−N3−C8	125.27(15)
C2−N1−C5	109.19(14)	C4−C5−N1	106.89(15)
C2−N1−C6	126.44(16)	C5−N1−C6	124.32(16)
C2−N3−C4	109.21(14)	C5−C4−N3	107.00(15)
C2−N3−C8	125.51(15)	O9−C10−C10	112.7(2)
N3−C2−N1	107.70(15)		

Figures

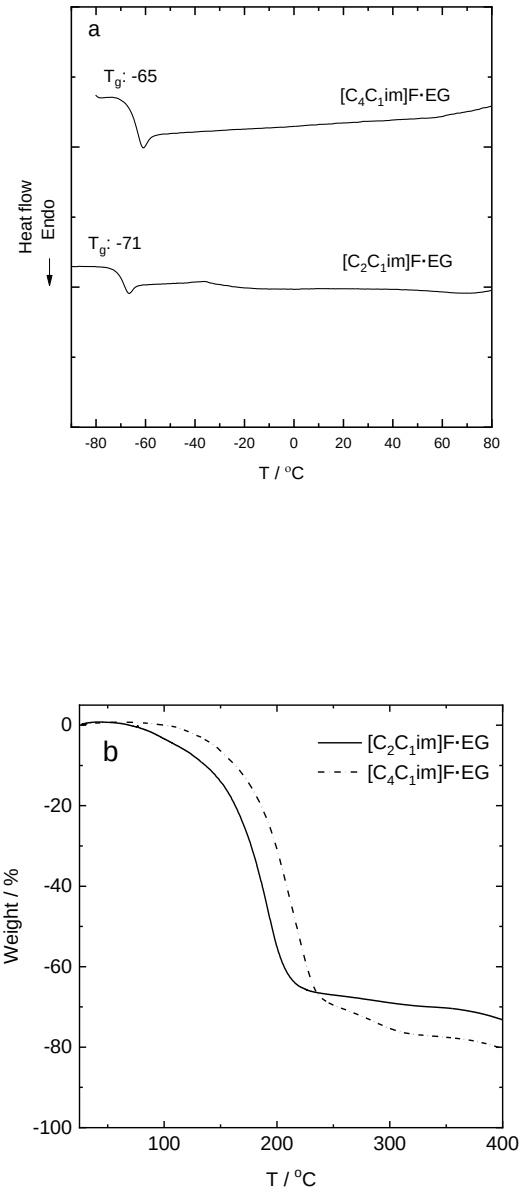

Fig. S1. DSC curves for (a) [C_2C_1im]F·EG and [C_4C_1im]F·EG (starting from the liquid state) and (b) TGA curves for [C_2C_1im]F·EG and [C_4C_1im]F·EG. Scan rate: 5 °C min^{-1}. Atmosphere: Ar atmosphere.

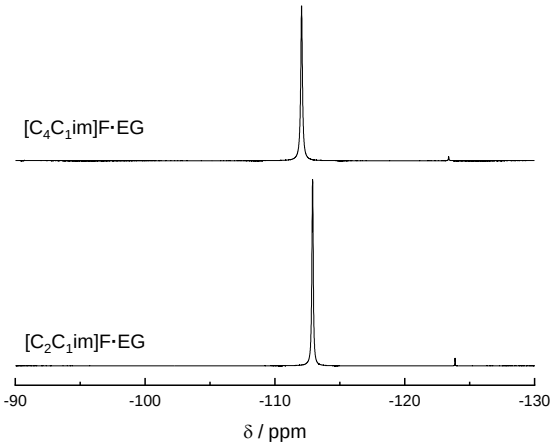

Fig. S2. ^{19}F NMR spectra of [C_2C_1im]F·EG and [C_4C_1im]F·EG at room temperature.

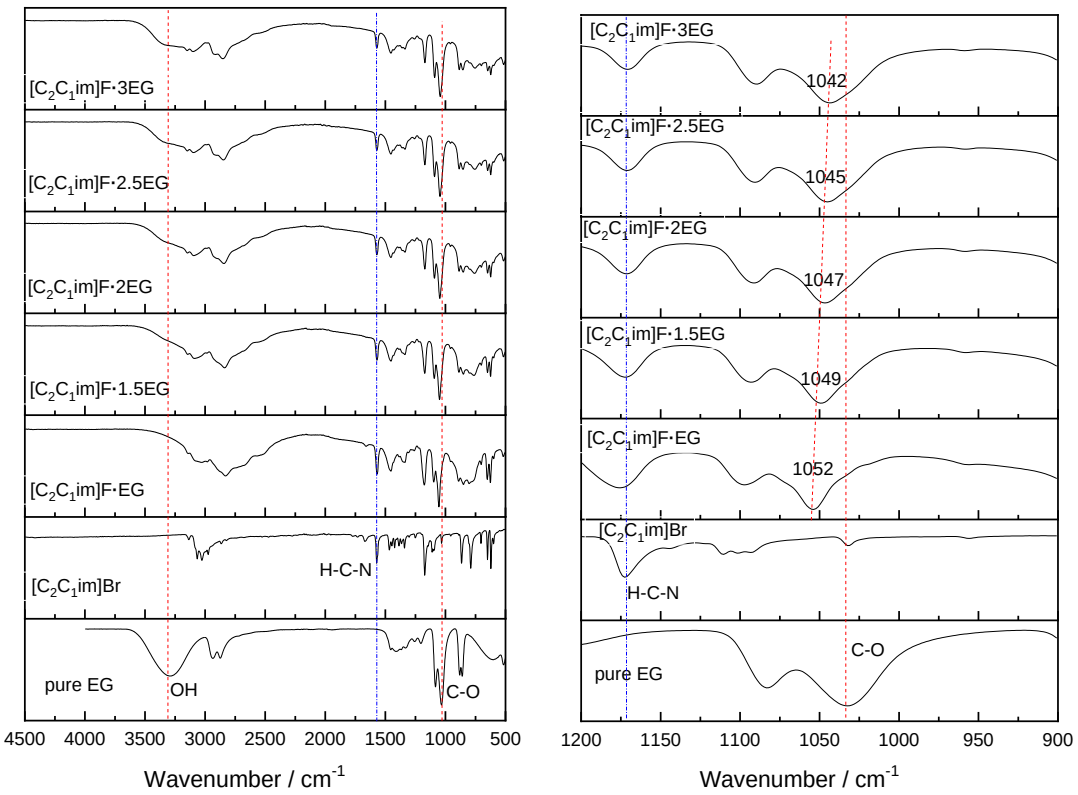

Fig. S3. IR spectra (full and local) of $[C_2C_1im]F{\cdot}EG$ with various EG amounts at 20°C, showing the shift of OH stretching and C-O stretching bands with increasing EG.

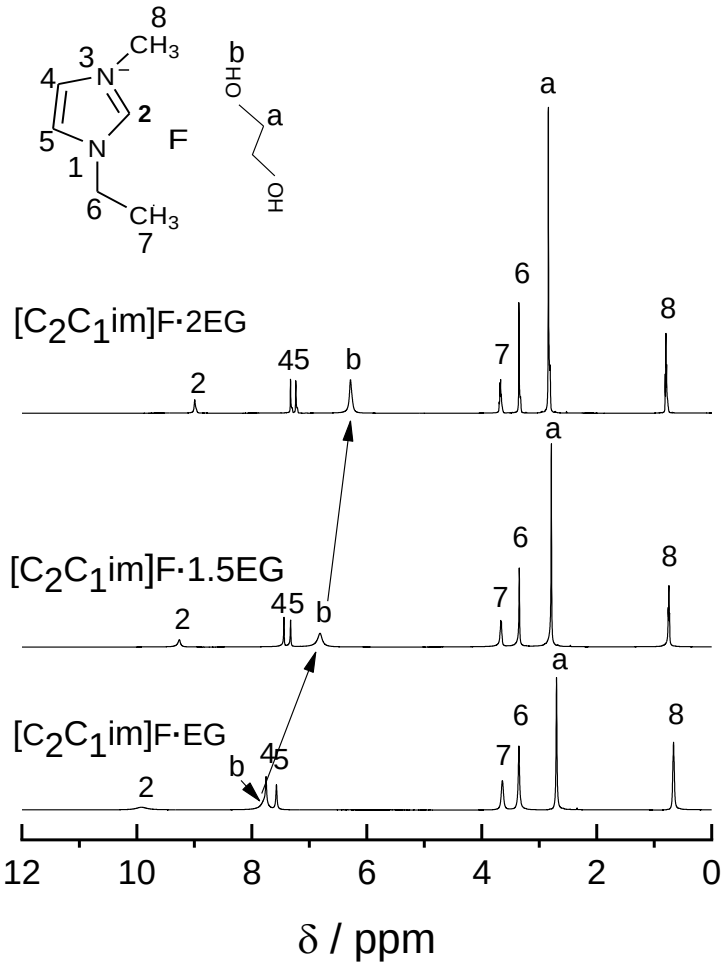

Fig. S4. ^{1}H NMR spectra of [C_2C_1im]F·*n*EG with various EG amounts at 20 °C.

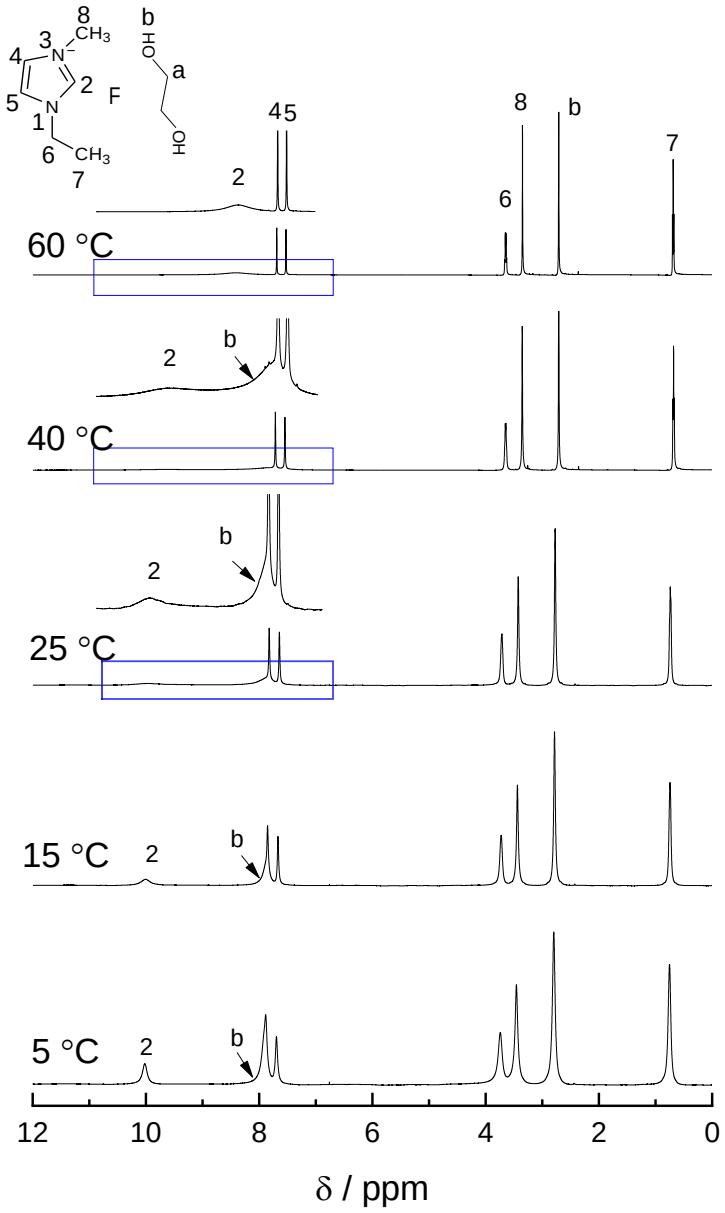

Fig.S5. ^{1}H NMR spectra of [C_2C_1im]F·EG at various temperatures from 5 °C to 60 °C.

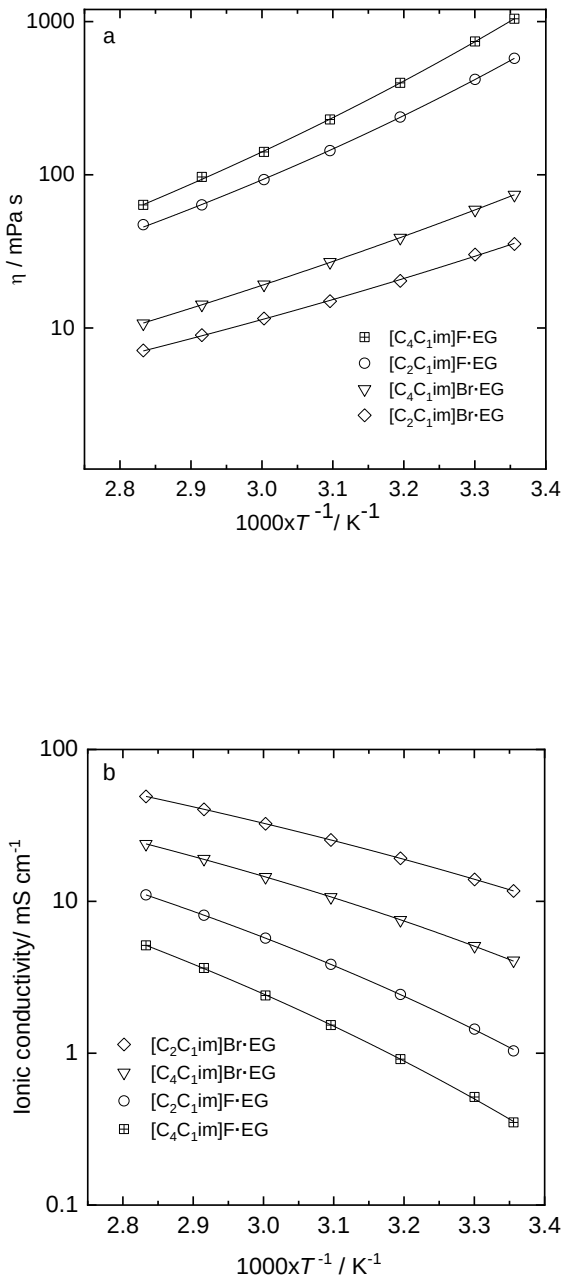

Fig. S6. Arrhenius plots of (a) viscosity and (b) ionic conductivity for [C_2C_1im]F·EG [C_4C_1im]F·EG, [C_2C_1im]Br-EG, and [C_4C_1im]Br-EG in the temperature range between 25 and 80 °C.

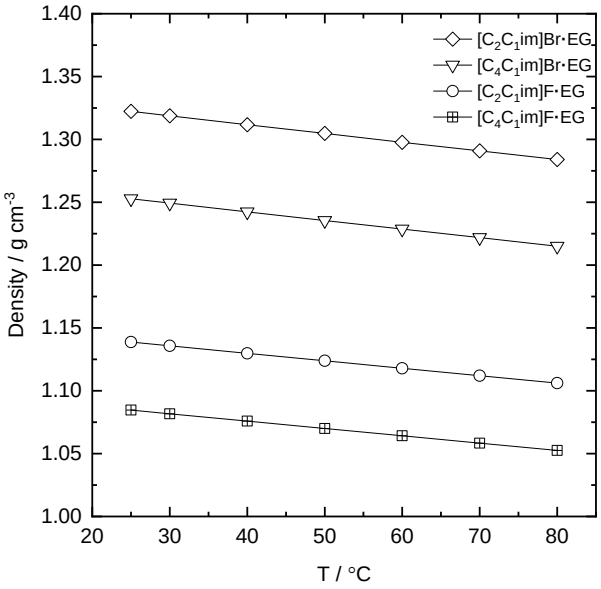

Fig. S7. Density data for $[C_2C_1im]F{\cdot}EG$, $[C_4C_1im]F{\cdot}EG$, $[C_2C_1im]Br$-EG, and $[C_4C_1im]Br$-EG in the temperature range between 25 and 80 °C.

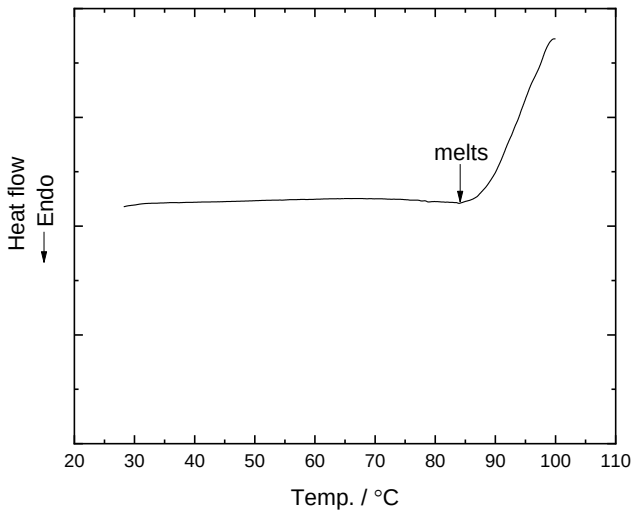

Fig. S8. DSC curves for $([C_2C_1im]F)_2 \cdot EG$ crystal.

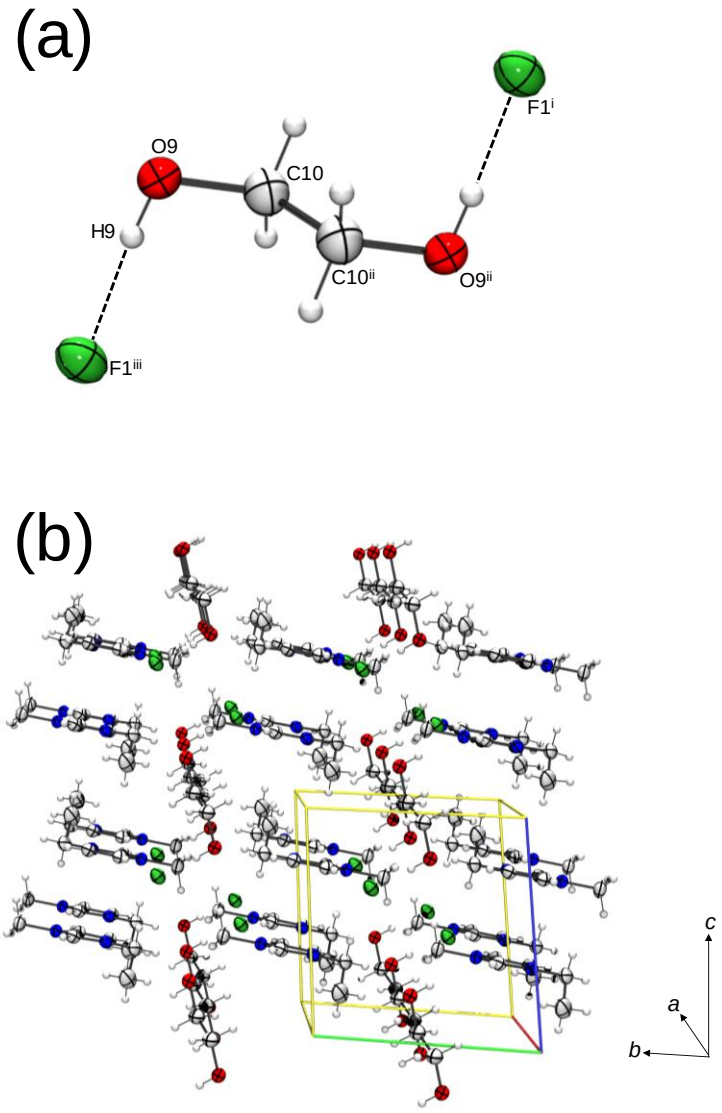

Fig. S9. (a) Conformation of EG molecule and (b) packing diagram for the $([C_2C_1im]F)_2 \cdot EG$ crystal structure.

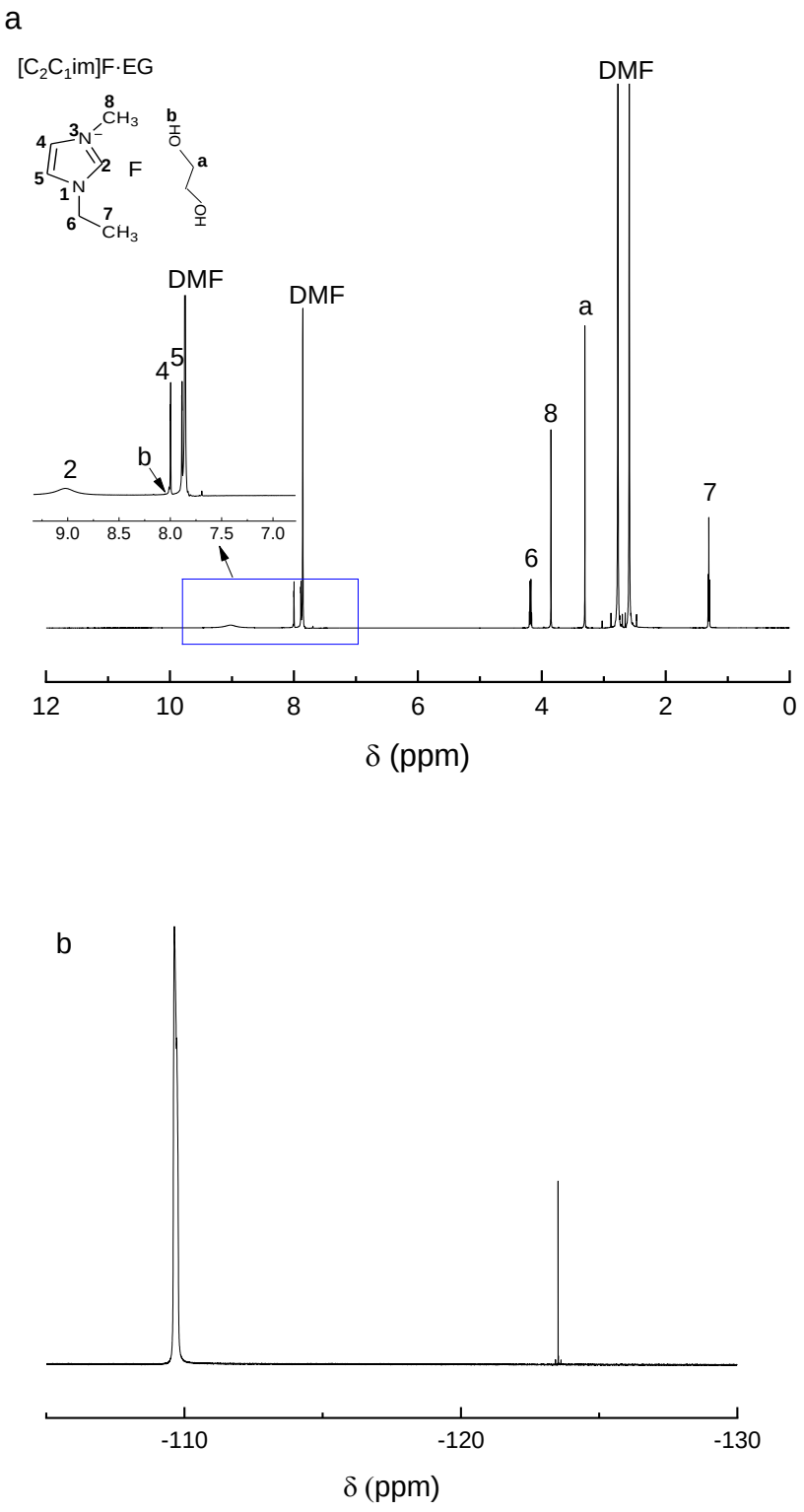

Fig. S10. (a) ^{1}H-NMR and (b) ^{19}F-NMR spectra of $[C_2C_1im]F{\cdot}EG$ in DMF at room temperature. The F impurity at 124 ppm in (b) is less than 0.4 %.

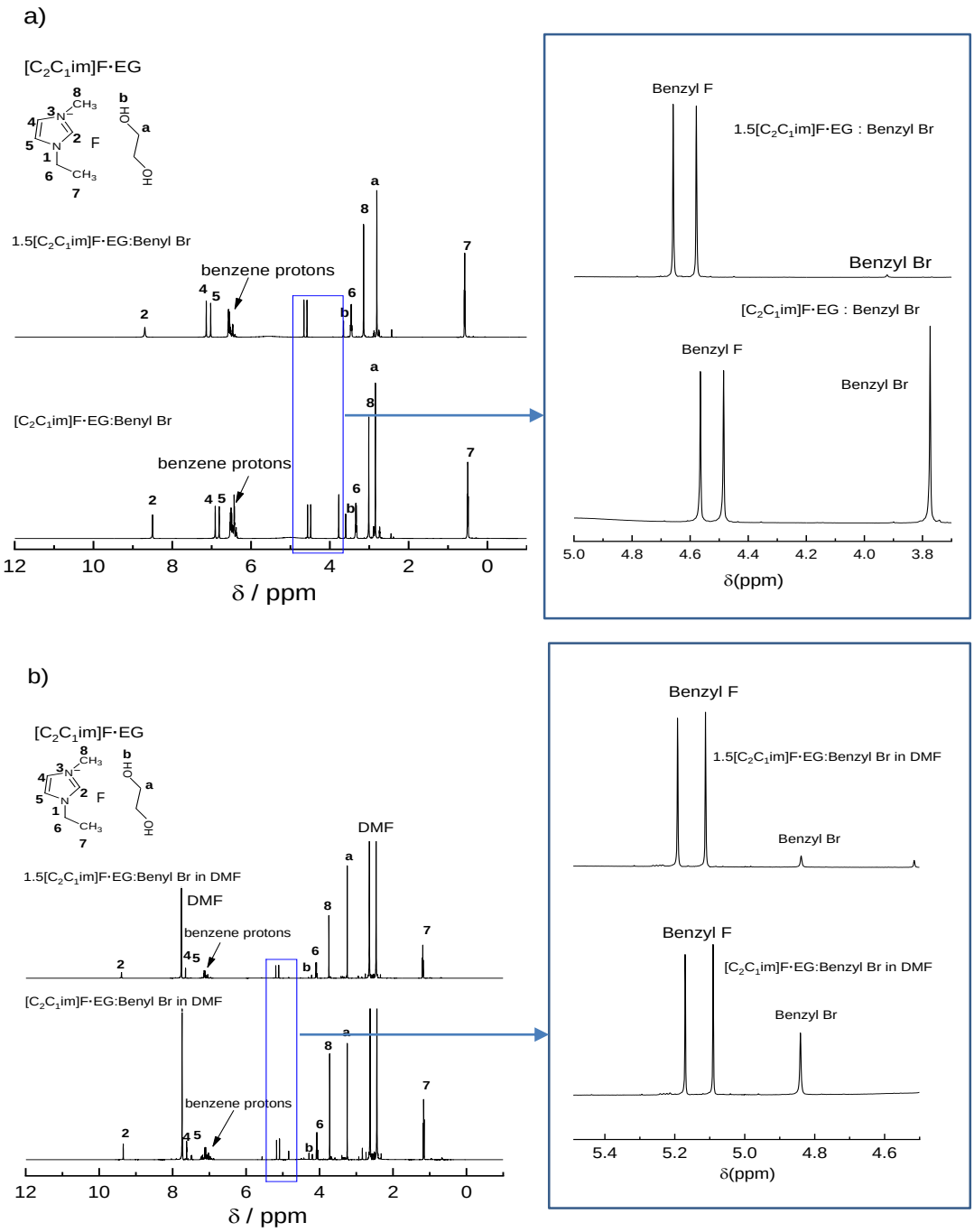

Fig. S11. ^{1}H-NMR of the products by the reaction of benzyl bromide with $[C_2C_1im]F{\cdot}EG$ at room temperature at two different F to Br ratios after stirring for two hours: (a) neat mixtures and (b) in DMF solvent. The enlarged areas on the right show the characteristic peaks for benzyl bromide and benzyl fluoride.

a)

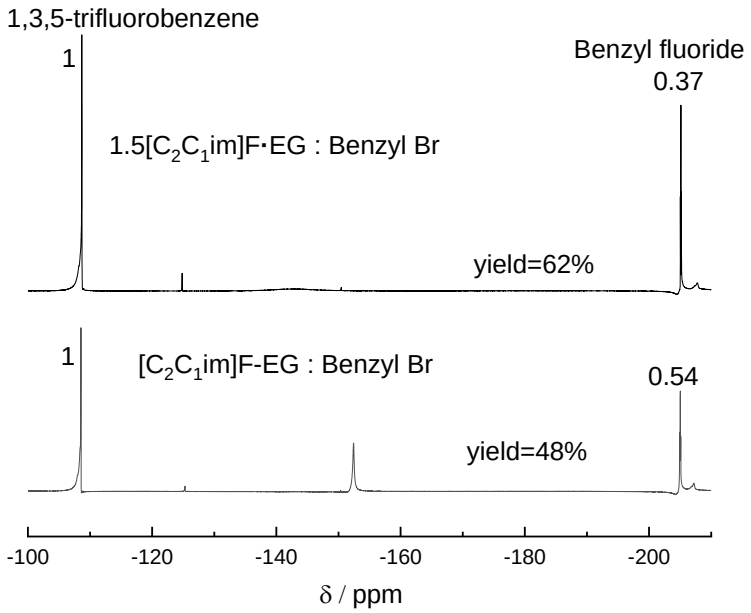

b)

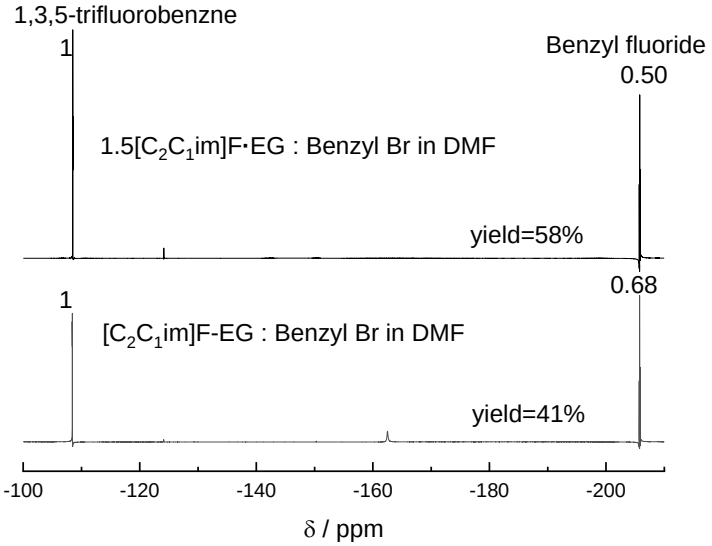

Fig.S12. ^{19}F-NMR of the products by the reaction of benzyl bromide with $[C_2C_1im]F{\cdot}EG$ at room temperature at two different F to Br ratios after stirring for two hours: (a) neat mixtures and (b) in DMF solvent. 1,3,5-trifluorobenzene was added as internal standard.

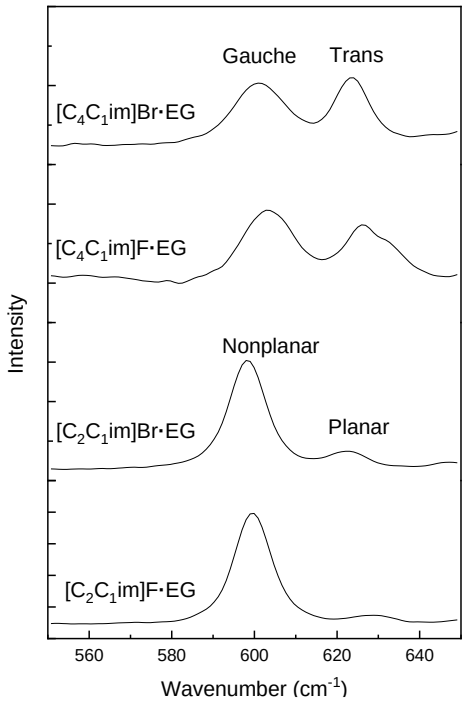

Fig.S13. Raman spectra of $[C_2C_1im]F{\cdot}EG$, $[C_2C_1im]Br{\cdot}EG$, $[C_4C_1im]F{\cdot}EG$, and $[C_4C_1im]Br{\cdot}EG$ at 20°C in the range between 550 and 650 cm^{-1}.

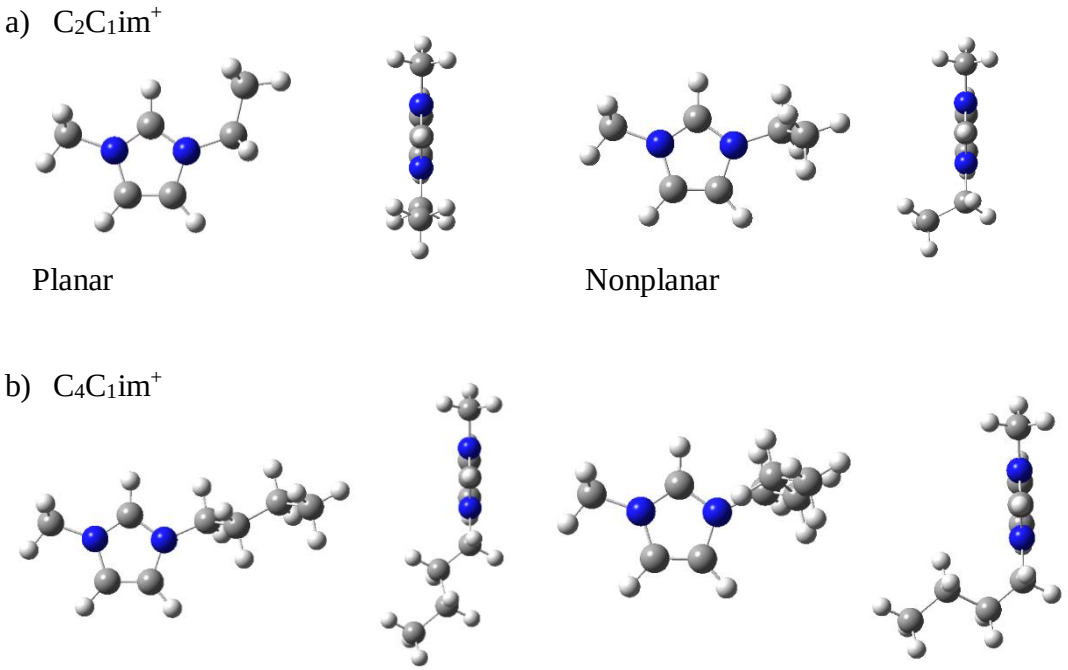

Fig.S14. Possible conformations of (a) $C_2C_1im^+$ and (b) $[C_4C_1im]^+$.

References

1. Price, W. S., Pulsed-Field Gradient Nuclear Magnetic Resonance as A Tool for Studying Translational Diffusion: Part 1. Basic Theory. *Concepts in Magnetic Resonance* **1997,** *9*, 299-336.
2. *RAPID AUTO, version 2.40*, Rigaku Corporation: Tokyo, Japan, 2006.
3. Altomare, A.; Cascarano, G.; Giacovazzo, C.; Guagliardi, A., Completion and Refinement of Crystal Structures with SIR92. *J. Appl. Crystallogr.* **1993,** *26*, 343-350.
4. Sheldrick, G. M., A Short History of SHELX. *Acta Crystallographica Section A* **2008,** *64*, 112-122.
5. J., F. L., WinGX Suite for Small‐Molecule Single‐Crystal Crystallography. *J. Appl. Crystallogr.* **1999,** *32*, 837-838.
6. Elias, S.; Karton-Lifshin, N.; Yehezkel, L.; Ashkenazi, N.; Columbus, I.; Zafrani, Y., Synthesis, Characterization, and Reactivity of Thermally Stable Anhydrous Quaternary Ammonium Fluorides. *Org. Lett.* **2017,** *19*, 3039-3042.
7. Holomb, R.; Martinelli, A.; Albinsson, I.; Lassègues, J. C.; Johansson, P.; Jacobsson, P., Ionic Liquid Structure: the Conformational Isomerism in 1-Butyl-3-Methyl-imidazolium Tetrafluoroborate ([Bmim][BF4]). *J. Raman Spectrosc.* **2008,** *39*, 793-805.
8. Satoshi, H.; Ryosuke, O.; Hiro-o, H., Raman Spectra, Crystal Polymorphism, and Structure of a Prototype Ionic-liquid [bmim]Cl. *Chem. Lett.* **2003,** *32*, 498-499.
9. Singh, D. K.; Cha, S.; Nam, D.; Cheong, H.; Joo, S.-W.; Kim, D., Raman Spectroscopic Study on Alkyl Chain Conformation in 1-Butyl-3-methylimidazolium Ionic Liquids and their Aqueous Mixtures. *ChemPhysChem* **2016,** *17*, 3040-3046.
10. Umebayashi, Y.; Hamano, H.; Tsuzuki, S.; Canongia Lopes, J. N.; Pádua, A. A. H.; Kameda, Y.; Kohara, S.; Yamaguchi, T.; Fujii, K.; Ishiguro, S.-i., Dependence of the Conformational Isomerism in 1-n-Butyl-3-methylimidazolium Ionic Liquids on the Nature of the Halide Anion. *J. Phys. Chem. B* **2010,** *114*, 11715-11724.
11. Katsyuba, S. A.; Zvereva, E. E.; Vidiš, A.; Dyson, P. J., Application of Density Functional Theory and Vibrational Spectroscopy Toward the Rational Design of Ionic Liquids. *J. Phys. Chem. A* **2007,** *111*, 352-370.
12. Elaiwi, A.; Hitchcock, P. B.; Seddon, K. R.; Srinivasan, N.; Tan, Y.-M.; Welton, T.; Zora, J. A., Hydrogen Bonding in Imidazolium Salts and its Implications for Ambient-Temperature Halogenoaluminate(III) Ionic Liquids. *J. Chem. Soc., Dalton Trans.* **1995**, 3467-3472.